JOURNAL OF MATERIALS SCIENCE **34** (1999) 3591–3596

Effect of ultrasonic treatment on ripening of titanium oxalate salt from solution

HEE-LACK CHOI, CHAN PARK
Department of Materials Engineering, PuKyong National University, San 100, Yong-Dang Dong, Nam-Gu, Pusan, Korea
E-mail: choihr@pine.pknu.ac.kr

Titanium oxalate was precipitated by the addition of $TiO(NO_3)_2$ solution to an ethanol solution of oxalic acid and then ripened in the mother solution with/without ultrasound at various temperatures. The influence of various factors such as reaction temperature and ripening time, as well as the effect of ultrasonic treatment in the solution, was investigated. During the ripening reaction of the titanium oxalate, a new crystalline phase was found. The chemical formula and the crystal system of the new phase were as follows: (1) Chemical formula—$Ti_2O_2(C_2O_4)(OH)_2H_2O$, (2) Crystal system—orthorhombic with lattice constants of $a = 1.0503$ nm, $b = 1.5509$ nm, and $c = 0.9700$ nm. The treatment of ultrasound during the ripening reaction accelerated the dissolution rate of the initial precipitated particles, so that the formation of the crystalline phase was hastened.

1. Introduction

It is known that a precipitation reaction [1] which does not take place under normal conditions proceeds with the ultrasonic treatment [2], although the mechanism of the effect is not yet fully understood. Ultrasonic treatment of fluid may produce acoustic cavitation. Cavitation can be divided into three stages: (1) formation, (2) growth, and (3) implosive collapse [3]. In sonochemistry, the energy of ultrasound induced by cavitation is applied to chemical reactions and fine powder processing.

Oxalate precipitation is widely used in the synthesis of titanate raw materials. These oxalates are generally highly insoluble, and they form particles that are readily filtered from the liquid and easy to handle [4]. Titanium oxalates are often used as precursors for the preparation of titanium-based perovskite oxides such as $BaTiO_3$, $Pb(Zr,Ti)O_3$, etc [5]. Most researchers focus their attentions on oxides from the precursors, while the process of the precipitation reactions is scarcely reported.

On the other hand, it is essential, in order to better understand the effect, to learn the systems, in which the precipitation phenomena without ultrasound are well-known. In this mono-component system, which is fundamental for the multi-components systems containing the titanium oxalates, an enhancement of the reaction rate and a new reaction which does not follow a routine reaction path are expected with ultrasonic treatment. We have been exploring the possibility of sonochemical powder processing [6, 7], which involves the powder preparation via precipitation in solution under ultrasonic treatment.

In this work, the precipitation and ripening reactions are investigated. And the effects of ultrasonic treatment are also evaluated by comparing the ripening reactions which are done with/without ultrasound.

2. Experiments

The flow chart of the preparation sequence is shown in Fig. 1. As a starting material, 0.028 mol/l solution of $TiO(NO_3)_2$ [8] was prepared by dissolving titanium hydroxide in nitric acid. The titanium hydroxide precipitate was previously obtained by titration of ammonia solution to $TiCl_4$ solution and subsequent filtration. Titanium content in the $TiO(NO_3)_2$ solution was determined by gravimetric analysis. TiO_2 was used as a weighing form. $TiO(NO_3)_2$ solution was poured into 0.028 mol/l solution of $H_2C_2O_4$ in EtOH, and then agitated with a magnetic stirrer and kept at various temperatures. The merit of using a ethanol solution is that oxalic acid is easily dissolved in ethanol and oxalates of alkaline earths and titanium are almost insoluble in ethanol [9]. The precipitate was ripened in the mother solution at 40 and 60 °C for various periods, agitated with a magnetic stirrer. The ripened products were filtered and washed with pure ethanol several times, and then dried for 1.5 days in air at room temperature.

The products were evaluated by X-ray diffractometry, Thermogravimetry/Differential Thermal Analysis (TG/DTA), Scanning Electron Microscope (SEM) and Fourier Transform Infrared Spectroscopy (FT-IR). The average particle size was analyzed without the drying process. The components of the products were determined by various chemical analysis methods: (1) absorbed water—gravimetric analysis, (2) constitution water—Karl Fischer's Method, (3) $C_2O_4^{2-}$—potassium permanganate titration method and combustion-infrared spectroscopy, (4) NO_3^-—ion-

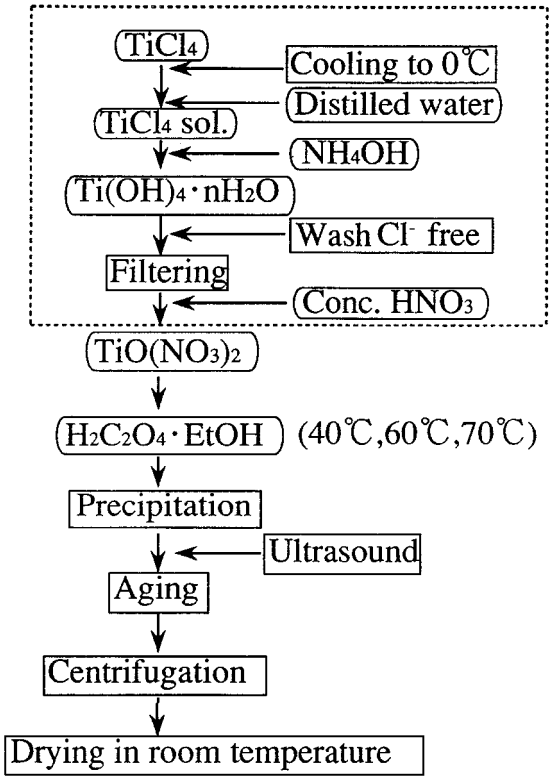

Figure 1 Flow chart of experiment.

exchange chromatography, (5) Ti—Hydrogen peroxide absorption spectrophotometry.

3. Results and discussion

3.1. Precipitates

When $TiO(NO_3)_2$ solution was poured into $H_2C_2O_4$-EtOH solution, white powder was precipitated. After 4 days of ripening at 40 °C, the powders was transformed to an unknown crystalline phase, which was named *Y-phase* in this paper. Its crystal system and lattice parameters will be described in the next section. No more changes were observed in the XRD patterns of the crystalline phase even after 15 days under this condition.

3.2. Ripening reaction

Fig. 2 shows X-ray diffraction patterns of the samples prepared from various ripening periods at 40 °C. The initial precipitate ripened for 1 day has a poor crystallinity. As the ripening time increases, the XRD pattern goes to the phase with good crystallinity. Fig. 3 shows scanning electron micrographs of these products. The precipitate of the 1 day exposure (Fig. 3a) consists of clusters of the particles, which disappear with the ripening time. On the other hand, the amount and size of the round shape particles also increase as ripening time increases (Fig. 3b). From these figures, it is believed that *Y-phase* was formed after the dissolution of the initial particles, which formed the clusters at first.

The result of the chemical analysis for the products ripened with various times is given in Table I. It can be seen that NO_3^- is contained in the initial precipitate, but

TABLE I Chemical analysis of the precipitates

	105 °C H_2O	800 °C H_2O	$C_2O_4^{2-}$	Ti	NO_3^-	TiO_2
Initial precipitate	18.6%	10.8%	30.1%	23.8%	4.0%	39.7%
Y-phase	6.5%	13.0%	32.6%	31.3%	0%	52.2%

105 °C H_2O (absorbed water)—Gravimetric analysis.
800 °C H_2O (constitution water)—Karl Fischer's Method.
$C_2O_4^{2-}$—Potassium permanganate titration method and combustion-infrared spectroscopy.
NO_3^-—Ion-exchange chromatography.
Ti—Hydrogen peroxide absorption spectrophotometry.

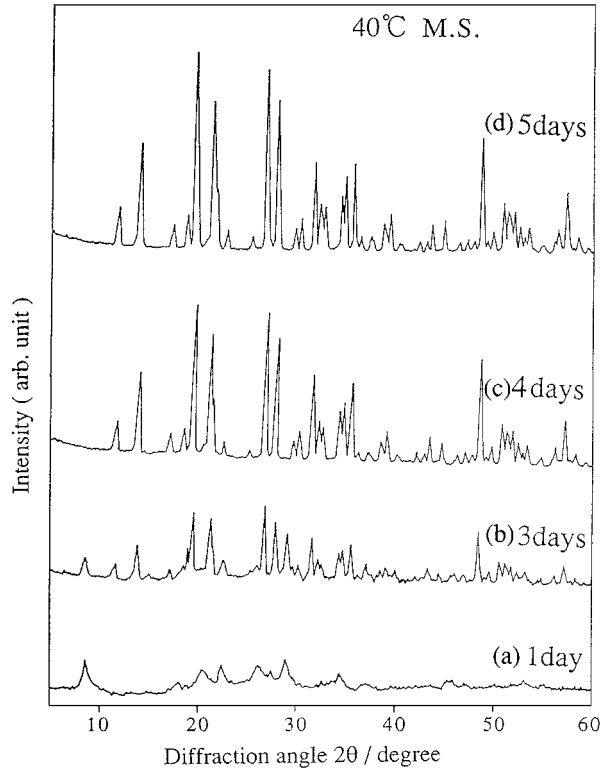

Figure 2 X-ray diffraction patterns of the precipitates with various ripening times at 40 °C: (a) 1 day, (b) 3 days, (c) 4 days, (d) 5 days.

not in the crystal. The initial precipitate has more absorbed water than the crystal, and the ratio of titanium to oxalate is different from that of other two samples. Judging from these results, it is obvious that the reaction is not a phase transformation reaction between the allotropes, but a dissolution-precipitation reaction.

X-ray diffraction patterns of the samples at 60 °C are given in Fig. 4. As ripening temperature increases, the time required for the formation of the crystal is shortened.

3.3. Characterization of Y-phase

From chemical analysis in Table I, *Y-phase* seems to be a titanium salt which contains $C_2O_4^{2-}$ and OH^-. As shown in Fig. 5, the DTA of Y-phase shows two endothermic peaks at 120 and 250 °C, and two exothermic peaks at 300 and 390 °C. Fig. 6 shows XRD pattern of Y-phase quenched from various temperatures. The pattern of Y-phase remained unchanged by heating below 180 °C. When heated to temperature between

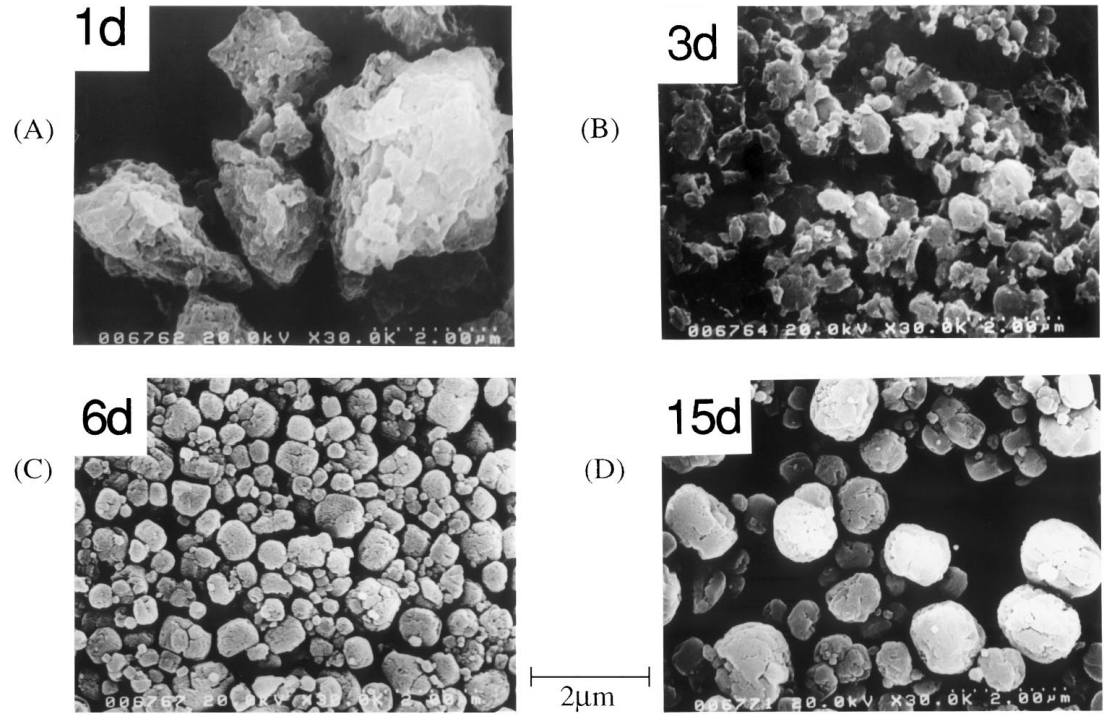

Figure 3 Scanning electron micrographs of the precipitates at 40 °C: (a) 1 day, (b) 3 days, (c) 6 days, (d) 15 days.

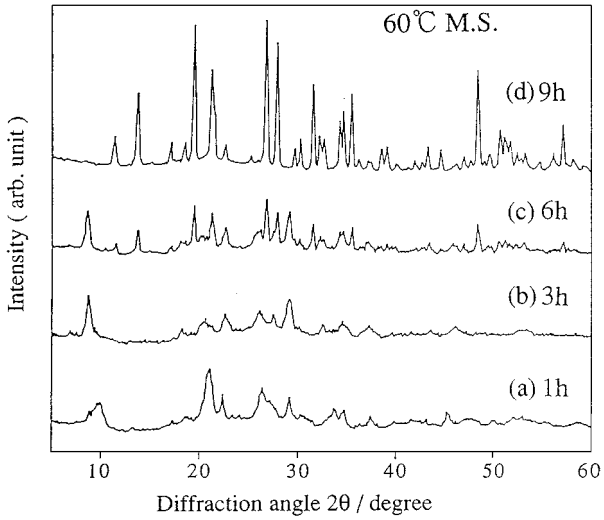

Figure 4 X-ray diffraction patterns of the precipitates with various ripening times at 60 °C: (a) 1 h, (b) 3 h, (c) 6 h, (d) 9 h.

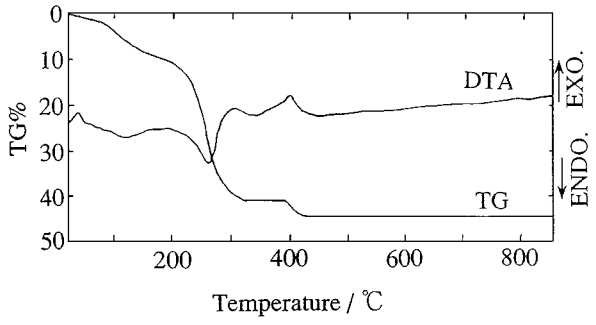

Figure 5 TG/DTA curves of Y-phase.

310 and 380 °C, the material showed an amorphous state. Heat treatment above 410 °C showed the anatase-type titanium dioxide. The attribution of each peak in the DTA curve is as follows; 120 °C—the evaporation of absorbed water, 250 °C—the breakdown of oxalate

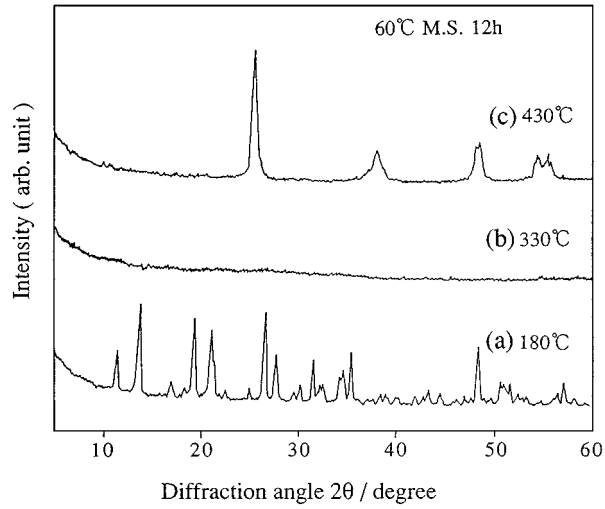

Figure 6 X-ray diffraction patterns at various temperatures: (a)180 °C, (b) 330 °C, (c) 430 °C.

and constitution water, 300 °C—the combustion of carbon monoxide, and 390 °C—crystallization to anatase. About 30% weight loss between 200 and 310 °C was contributed to the breakdown of the constitution water and oxalate into carbon dioxide and monoxide. Fig. 7 illustrates the FT-IR spectra of the material. With the band at 1700 cm^{-1}, which is ascribed to C=O, the presence of $C_2O_4^{2-}$ is predicted [10]. The high wave numbers, 3100–3650 cm^{-1}, show the bands due to the presence of water. The sharp band at 3600 cm^{-1} is stretching vibration of constitution water. The broad band at 3200 cm^{-1} is deformation vibration of hydration water. And it can be thought that the material contains the two types of water. The water below 150 °C was excluded as an adsorption water.

With the result of chemical analysis, molecular ratio was determined to be 2 : 1.12 : 2.18 from the weight ratio of Ti, C_2O_4, H_2O over 105 °C, respectively. From

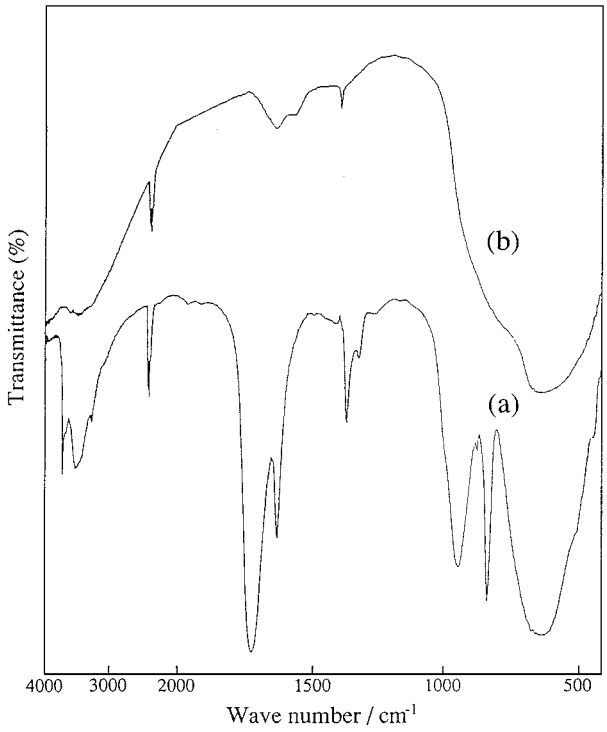

Figure 7 FTIR spectra of Y-phase at various temperatures: (a) room temperature and (b) 330 °C.

the result of TG, one mole of water (about 7%) which does not affect the structure exists at temperatures between 105 and 180 °C. With X-ray diffraction analysis it was known that the structure did not change with temperature up to 180 °C. Adjusting the electrical neutrality with oxygen, we assumed that the chemical formula of the crystal is $Ti_2O_2(C_2O_4)(OH)_2 \cdot H_2O$.

The calculation of the density was used for the following formula.

$$\rho = \sum \frac{A}{NV} = \sum \frac{A}{(6.02257 \times 10^{23}) \times (V \times 10^{-21})}$$
$$= 1.66042 \times 10^{-3} \times \sum \frac{A}{V} = \frac{ZM}{V} \quad (1)$$

ρ: density, N: Avogadro number, V: Volume of a unit cell by nm^3, $\sum A$: Sum of atomic weight in a unit cell (for the compound, $\sum A = ZM$, Z: The number of molecular in a unit cell, M: Molecular weight).

The density of Y-phase measured with an picnometer was 2.21 g/cm^3. The volume of a unit cell calculated from lattice constants was 1.58 nm^3, and the molecular weight of the Y-phase was 267.82. With these values, Z could be determined. Because Z value is usually an integer except for the material which has a structural defect, it is determined to be 8. The theoretical density calculated from above Equation 1 was 2.25 g/cm^3.

The absorbed bands at 1650–1700 cm^{-1}, which is the vicinity of carbonate band range [10] shown FT-IR spectrum of the Y-phase at 330 °C in Fig. 7b were not clearly identified yet. It is confirmed that the constitution water bands in the Y-phase were completely disappeared at 330 °C. It is suggested that the material of the amorphous state between 310 and 380 °C is a kind of carbonate formed from the breakdown of

TABLE II Experimental conditions

Radiation type, source, power	X-ray, Cu, 40 kV and 30 mA
Wavelength	1.5406 Å(K_α)
Discriminator	monochromator
Detector	scintillation counter
Instrument description	17 cm radius, vertical diffractometer Philips PW 1050/25
Divergence angle	1°
Receiving-slit width	0.2 mm
Temperature	room temperature
External 2θ standard	Si ($a_0 = 5.43075$ Å)
Range of 2θ	from 4° to 70°
Scan technique	step-scanning, step size = 0.01°
Specimen preparation	packed

oxalate. Observation of Y-phase by SEM showed that the grains exhibited an oval shape of approximately several micrometers in size with a slightly convoluted surface (Fig. 3d). X-ray diffraction data of the powder sample were collected at room temperature using a Philips PW1700 diffractometer (Table II). Powder diffraction data are given in Table III. The data were indexed on an orthorhombic unit cell using the program ITO [11]. Systematic absences suggest that the space group is $C222_1$; $hkl: h + k = 2n$, $h0l: h = 2n$, $h00: h = 2n$, $00l: l = 2n$, $0kl: k = 2n$, $hk0: h + k = 2n$, $0k0: k = 2n$. More confirmable works are needed for a verification. Lattice constants were refined by the least-squares method from 31 reflections using the program RCL3 [12]. The figure of merit M20 defined by de Wolff [13] was 43.6 suggesting reliable indexing. Fig. 8 shows TEM micrograph and the electron diffraction pattern. The diffraction pattern coincides with the orthorhombic lattice.

3.4. Ultrasonic treatment

The emitting titanium horn was dipped into the liquid as shown in Fig. 9. Ultrasound of 20 kHz with an acoustic intensity of 1.9 W/cm^2, was applied just after the initial precipitates appeared. The precipitates continued to be ripened in the mother solution with ultrasound after that. This has nothing to do with initial precipitation reactions. The power of ultrasonicator was calorimetrically estimated by an adiabatic measurement of the temperature rise in water exposed to the ultrasound. The temperature of the reaction chamber was kept constant by using a cooling-circuit to exclude the influence of the temperature rise caused by the ultrasound.

Fig. 10 shows the X-ray patterns of the ripening products obtained by ultrasonic treatment at 60 °C. The formation of Y-phase was completed after 6 hours of ripening with ultrasound, while it had just begun to form after 6 hours of ripening without ultrasound at 60 °C (Fig. 4). The effects of the ultrasound and the reaction temperature on the ripening reaction are summarized in Table IV. In this reaction, the ultrasonic treatment effectively promoted the ripening process; in other words, it extremely hastened the formation of Y-phase. The reaction of this system proceeds through three stages: (1) precipitation of the initial particles; (2) dissolution of the initial particles; (3) formation of Y-phase. It can be considered that the acceleration of the formation of

TABLE III X-ray diffraction data of Y-phase

hkl	2θ obs	I/I_0	dobs	dcalc	$\Delta 2\theta$	*hkl*	2θ obs	I/I_0	dobs	dcalc	$\Delta 2\theta$
020	11.39	24	7.763	7.755	0.012	243	40.11	2	2.246	2.245	0.023.
111	13.65	65	6.482	6.475	0.014	333	41.83	4	2.158	2.158	−0.009
200	16.86	12	5.254	5.251	0.010	441	42.60	3	2.121	2.121	−0.018
002	18.25	19	4.857	4.850	0.027	171	42.70	2	2.116	2.116	0.008
201	19.19	90	4.621	4.618	0.014	262	43.20	10	2.092	2.092	0.002
220	20.38	5	4.354	4.348	0.028	403	44.42	12	2.038	2.038	−0.011
112	20.93	62	4.241	4.236	0.025	423	46.01	4	1.971	1.971	−0.005
131	21.19	26	4.189	4.185	0.025	080	46.85	6	1.938	1.939	−0.022
022	21.58	1	4.115	4.112	0.013	512	47.49	4	1.913	1.913	0.003
221	22.36	7	3.973	3.968	0.029	263	48.26	44	1.884	1.885	−0.005
040	22.91	1	3.879	3.877	0.008	334	48.94	4	1.860	1.860	−0.010
202	24.94	5	3.567	3.563	0.031	460	49.46	6	1.841	1.842	−0.016
132	26.57	100	3.352	3.352	−0.001	532	50.51	18	1.806	1.806	−0.013
311	27.67	78	3.221	3.221	0.001	135	50.95	10	1.791	1.790	0.033
241	30.07	16	2.969	2.969	0.000	404	51.26	15	1.781	1.781	−0.016
151	31.42	45	2.845	2.844	0.009	064	51.66	15	1.768	1.769	−0.015
312	32.00	14	2.795	2.792	0.028	513	52.24	9	1.750	1.750	−0.012
203	32.49	21	2.754	2.753	0.003	424	52.69	6	1.736	1.736	−0.018
133	33.74	1	2.654	2.653	0.024	462	53.16	9	1.722	1.722	−0.016
242	34.13	26	2.625	2.624	0.019	315	54.37	1	1.686	1.687	−0.023
223	34.54	36	2.595	2.595	0.000	191	54.74	2	1.676	1.675	0.020
004	37.04	6	2.425	2.425	0.000	245	55.75	2	1.647	1.647	0.002
421	37.26	3	2.411	2.409	0.036	552	56.16	9	1.637	1.637	−0.021
313	38.26	7	7.351	2.348	0.044	155	56.56	2	1.626	1.625	0.031
114	38.51	9	2.336	2.336	−0.002	335	57.01	23	1.612	1.612	−0.016
024	38.89	11	2.314	2.315	−0.012	463	57.55	2	1.600	1.601	−0.012
402	38.99	10	2.308	2.309	−0.015	283	58.16	4	1.585	1.585	−0.013
351	39.87	2	2.260	2.258	0.030	026	58.28	3	1.582	1.583	−0.030

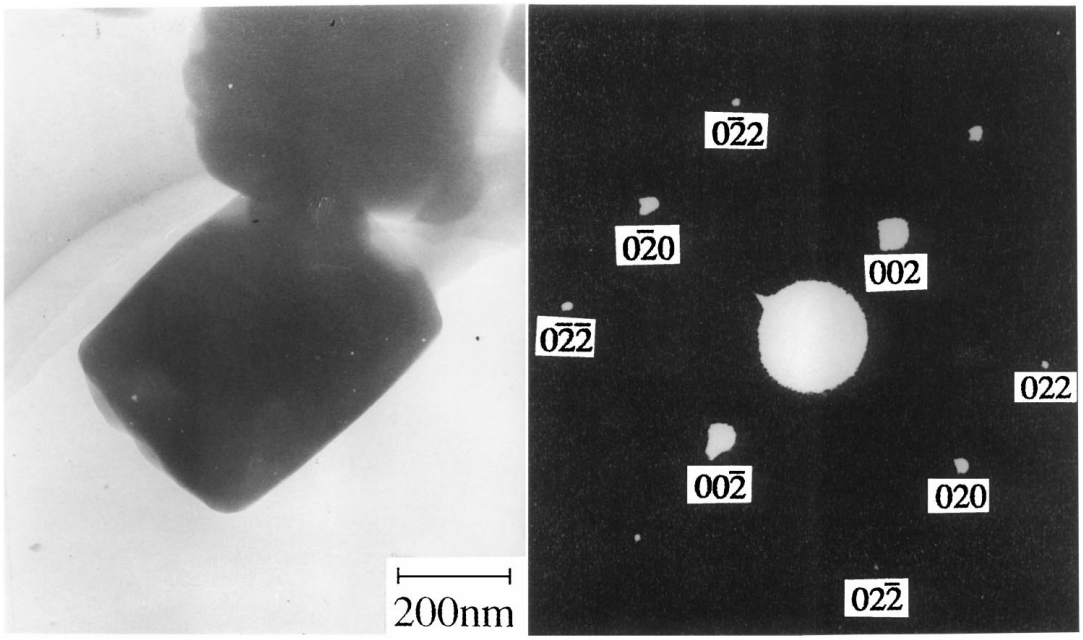

Figure 8 Tem micrograph (left) and the electron diffraction pattern (right) of Y-phase.

Y-phase is due to the promotion of the dissolution of the initial particles by ultrasonic treatment. And the promotion by ultrasonic treatment is ascribed to the following effects:

(1) The effect of increasing surface area of the precipitates by the action of bubble collapse; The average secondary particle sizes of the powders ripened for one hour with and without ultrasonic treatment are approximately 3 μm (U.S.) and 9 μm (M.S.) respectively. The powders were not dried before measuring particle sizes. It is concluded that ultrasound is responsible for the dispersion of the initial particles by the difference of average partilce size.

(2) The effect of the microstream generated by the vibration of bubble.

(3) The effect of the dance of particles in the mother solution by a straight flow generated by ultrasonic wave pulse.

The ripening reaction is further accelerated by increasing input power. It is obvious that the cavitation,

TABLE IV Apperance and occupation of Y-phase with various ripening conditions

Ripening condition	Appearance of Y-phase	Occupation of Y-phase
40 °C, M.S.	48 h	96 h
60 °C, M.S.	6	9
70 °C, M.S.	2	4
60 °C, 20 kHz (1.9 W/cm^2)	2	4
60 °C, 20 kHz (25.4 W/cm^2)	<1	<1
70 °C, 20 kHz (1.9 W/cm^2)	1.5	2.5

M.S.: Mechanical Stirring.

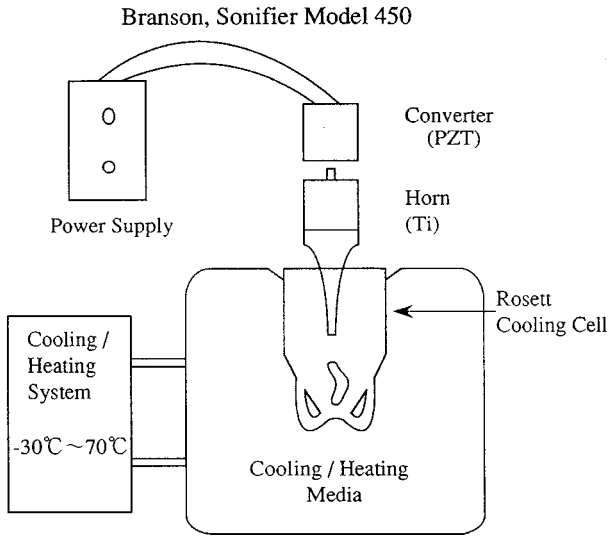

Figure 9 A schematic illustration of the apparatus.

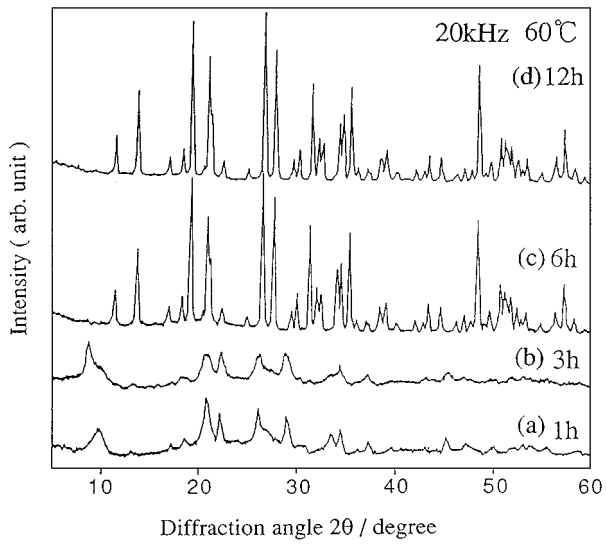

Figure 10 X-ray diffraction patterns of the precipitates with various ripening times at 60 °C, 20 kHz ultrasound (a) 1 h, (b) 3 h, (c) 6 h, (d) 12 h.

which is the origin of ultrasound energy in liquid state becomes more active with the input power [14], so that the enhancement of dissolution occurs.

4. Conclusions

The initial precipitate has a poor crystallinity and contains NO_3^- as well as $C_2O_4^{2-}$. Ripening changes this precipitate to a crystalline phase. The crystalline phase has the chemical formula $Ti_2O_2(C_2O_4)(OH)_2 \cdot H_2O$. The crystal system is orthorhombic with lattice constants of $a = 1.0503$ nm, $b = 1.5509$ nm and $c = 0.9700$ nm. It was found that the treatment of ultrasound during the ripening reaction accelerated the dissolution rate of the initial particles, so that the formation of the crystalline phase was hastened.

Acknowledgement

The authors appreciate Mr. T. Sato of Analysis Center Company Limited for the chemical analysis of the precipitates and Professor N. Ishizawa of Tokyo Institute of Technology for providing the software used in the cell-finding calculation.

References

1. Y. FANG, D. K. AGRAWAL, D. M. ROY and P. W. BROWN, *J. Mater. Res.*, **7** (1992) 2294–2298.
2. K. S. SUSLICK and GAWIENOWSKI, *J. Phys. Chem.* **87** (1983) 2299.
3. *Idem., Science* **23**, (1990) 1429–1445.
4. M. R. D. GUIRE and W. B. PHILIPP, *J. Mater. Chem.* **3**, (1993) 571–574.
5. Y. ENOMOTO and A. YAMAJI, *J. Amer. Ceram. Soc. Bull.* **60** (1981) 566–570.
6. H. L. CHOI, N. ENOMOTO and Z. NAKAGAWA, in Proceedings of the 9th Korean-Japan Seminar on new Ceramics, Korea Kyoungju December 1992, pp. 125–129.
7. Y. TOMOMASA, N. ENOMOTO, Y. OHYA and Z. NAKAGAWA, in Proceedings of the MRS International Meeting on Advanced Materials, Tokyo, May 1988, Vol. 3, pp. 107–114.
8. H. L. CHOI and Z. NAKAGAWA, *J. Mater. Sci.* **29** (1994) 3239–3242.
9. H. YAMAMURA, A. WATANABE, S. SHIRASAKI, Y. MORIYOSHI and M. TANADA, *Ceramics International* **11** (1985) 17–22.
10. L. J. BELLAMY, "The Infrared Spectra of Complex Molecules" (Chapman and Hall, London, 1980).
11. J. W. VISSER, *J. Appl. Crystallogr.* **2** (1969) 89.
12. T. SAKURAI, "Universal Program for Crystallographic Computation" Cryst. Soc. Jpn. (1967)
13. DE WOLFF, P. M., *J. Appl. Crystallogr.* **1** (1968) 108.
14. V. M. FRIDMAN, *Ultrasonics*, July (1972) 162–165.

Received 28 September 1998
and accepted 11 February 1999